




Noninvasive and real-time monitoring of Au nanoparticle promoted cancer metastasis using in vivo flow cytometry

WEN PANG,^{1,5} SHIHUI DING,^{1,5} LIYUN LIN,¹ CHEN WANG,¹ MAN LEI,¹ JIALE XU,¹ XINTONG WANG,¹ JUNLE QU,² XUNBIN WEI,^{1,3,4} AND BOBO GU^{1,*} 

¹School of Biomedical Engineering, Shanghai Jiao Tong University, Shanghai 200030, China

²Key Laboratory of Optoelectronic Devices and Systems of Ministry of Education and Guangdong Province, College of Physics and Optoelectronic Engineering, Shenzhen University, Shenzhen 518060, China

³Biomedical Engineering Department, Peking University, Beijing 100081, China

⁴Key Laboratory of Carcinogenesis and Translational Research (Ministry of Education/Beijing), Peking University Cancer Hospital & Institute, Beijing, 100142, China

⁵Contributed equally to this work

*bobogu@sjtu.edu.cn

Abstract: Cancer is the second leading cause of mortality globally, while cancer metastasis, which accounts for about 90% of cancer-related mortality, presents an extremely poor prognosis. Thus, various nanomedicines were designed and synthesized for cancer treatment, but nanomaterials could lead to endothelial leakiness and consequently facilitate intravasation and extravasation of cancer cells to form circulating tumor cells (CTCs), which were regarded as the potential metastatic seeds, possibly accelerating cancer metastasis. Neither possible metastatic sites were observed nor rare CTCs could be measured using common methods at the early stage of cancer metastasis, it is urgent to explore new technology to dynamically monitor nanomedicine promoted cancer metastasis with high sensitivity, which would be beneficial for cancer treatment as well as design and synthesis of nanomedicine. Herein, a novel optical biopsy tool i.e. in vivo flow cytometry (IVFC) was constructed to noninvasively and real-time monitor CTCs of tumor-bearing mice treated with various concentrations of Au nanoparticles. The in vivo experimental results demonstrated the promoted CTCs were Au nanoparticles dose-dependent consistent with the in vitro results, which showed Au nanoparticles induced dose-dependent gaps in the blood vessel endothelial walls to accelerate CTCs formation, making IVFC a promising biopsy tool in fundamental, pre-clinical and clinical investigation of nanomedicine and cancer metastasis.

© 2021 Optical Society of America under the terms of the [OSA Open Access Publishing Agreement](#)

1. Introduction

Cancer is one of the major diseases threatening human health worldwide. According to the latest global cancer data from the World Health Organization (WHO), more than 18.1 million new cases and 9.6 million death cases have been reported worldwide in 2018, making cancer one major public health issue [1]. In addition to the conventional cancer treatment methods including surgery, chemotherapy, and radiotherapy, various emerging cancer treatment modalities have been proposed and demonstrated such as photodynamic therapy (PDT), photothermal therapy (PTT), gene therapy, etc [2–4]. Since approved for clinical use, these emerging cancer treatment methods are developing new strategies to further improve therapeutic outcomes. In order to further improve reactive oxygen species (ROS) generation capability and consequently PDT efficiency, many new photosensitizers including fluorogens with aggregation-induced emission (AIE) characteristics (AIEgens) [5], graphene quantum dots (QDs) [6], black phosphorus [7],

carbon dots [8], etc., have been designed and synthesized for PDT applications. Meanwhile, novel PTT agents with high photothermal effect, including semiconducting polymer nanoparticles (NPs) [9], gold NPs [10], melanin NPs [11], were applied to enhance anticancer efficiency. Moreover, many recently developed nanocarriers, such as two-dimensional materials [3] and silica NPs [12], were functionalized to realize gene delivery and consequently high-performance gene therapy. The rapid development of nanotechnology paves the way to improve survival rate and lifetime of most cancer patients [13], but the toxicity of these nanomaterials is still a major concern for translating them for clinical research. Recent studies demonstrated that some NPs could induce endothelial leakiness (NanoEL), which lowered the barrier for intravasation of surviving cancer cells into the surrounding vasculature to form circulating tumor cells (CTCs) and subsequently extravasate [14]. CTC is regarded as the potential metastatic seed. It means that NanoEL can accelerate metastasis, which actually accounts for the vast majority of cancer-related mortality (~90%) [15]. It is extremely important to monitor the CTCs promoted by NanoEL at the early state, which benefits for the understanding of the behavior of NPs in complex biological media and especially optimizing nanomedicine for cancer treatment.

With the advances of multidisciplinary studies, CTC detection methods are under rapid development. CellSearchs (Veridex, Raritan, NJ) is the first and only product approved by the U.S. food and drug administration (FDA) for detecting CTCs in 2004, but it also suffers from some limitations e.g. the system is rather expensive, the sensitivity and selectivity are low, etc. CellCollectors (GILUPI GmbH, Potsdam, Germany) is a European Conformity approved medical device and is the first in vivo CTC isolation product worldwide, but the method is invasive, making it less accepted by patients. In order to overcome these limitations of CellSearchs and CellCollectors, many novel CTC detection methods have been proposed and demonstrated, most of which are based on in vitro analysis of the blood sample [16]. The CTC could be directly detected by the line-confocal microscope [17] and surface-enhanced Raman scattering (SERS) technology [18], but enriching process is commonly adopted due to that the CTC is extremely rare in the blood sample. Before enrichment, CTC should be captured, which can be realized with/without CTC-specific ligands [19,20]. Normally, ligand capture endows the CTC detection better performance [21]. Once captured, the CTCs are enriched by density gradient sedimentation, size exclusion filtration, barcode particles, self-propelled micromachines, magnetic beads, etc., and finally detected using fluorescence, electrical impedance, etc [16]. Although enrichment is also feasible in vivo, it is rather invasive [22].

The CTC detection methods mentioned above suffer from either complicated detection process or invasiveness. Meanwhile, the blood sampling process separates CTC from the practical physiological environment, possibly resulting in CTC changes and detection errors. Moreover, the detection sensitivity and dynamic monitoring are restricted due to the limited amount of blood and sampling frequency. Optical methods, featured with non-invasiveness, high sensitivity and resolution, show great potential in biopsy, e.g. in vivo endomicroscopy [23], in vivo confocal/two-photon microscopy [24,25], in vivo photoacoustic flow cytometry [26], in vivo fluorescence flow cytometry [27] and in vivo photoacoustic/fluorescence flow cytometry [28], have been used for CTC detection and monitoring CTC formation during cancer cells release from the tumor during radiotherapy [29], biopsy and surgery [30]. The in vivo flow cytometry (IVFC), which combines the advantages of traditional flow cytometry and in vivo confocal microscopy, can real-time and quantitatively detect circulating cells (including CTCs) in vivo without any processing of specimen [27], making it a good candidate to noninvasively and real-time monitor CTC promoted by NanoEL.

Herein, we constructed IVFC to noninvasively and real-time monitor the rare CTC in the early stage of metastasis, which can't be detected using conventional methods, making IVFC a promising biopsy tool to study the influence of nanoparticles on cancer metastasis. In vitro cellular experiments demonstrated that the Au nanoparticles could induce endothelial leakiness

by promoting gaps between endothelial cells and facilitate cancer cells to cross the endothelial barrier to form CTCs. Then the Au nanoparticles dose-dependent CTCs were noninvasively and real-time monitored using the proposed IVFC, indicating high dose of Au nanoparticles could promote cancer metastasis. When designing nanomedicine for future clinical use, IVFC is an indispensable tool to in vivo assess the nanomedicine effect.

2. Materials and methods

2.1. Materials

Sodium citrate and HAuCl_4 were purchased from Sinopharm Chemical Reagent Co., LTD. RPMI1640 medium and phosphate buffered saline (PBS, 1X) were purchased from HyClone. Bovine serum albumin (BSA) was purchased from Sigma. Edetic acid (EDTA) was purchased from BBI life sciences corporation. PC3 cells were gifted by Professor Weiqiang Gao at Shanghai Jiao Tong University. Fetal bovine serum (FBS) and endothelial cell medium (ECM) were purchased from ScienCell. Human microvascular endothelial cells (HMECs) were purchased from Shanghai Zhong Qiao Xin Zhou Biotechnology Co., LTD. Cell counting kit-8 (CCK-8) assay kit was purchased from Dojindo Laboratories. Puromycin was purchased from Gibco. Polybrene and pLVX-EGFP1-C1 were purchased from Takara Bio Company. Phalloidin (DyLight 554) was purchased from Cell Signaling Technology. Hanging cell culture inserts (8 μm , 24-well) were purchased from Corning. Light emitting diode (LED) was purchased from CCS Inc. Charge-coupled device (CCD) was purchased from Sony. Photomultiplier tube (PMT) was purchased from Hamamatsu. The filters and dichroic mirrors were purchased from Semrock. The objective lens was purchased from Olympus. The mirror, achromatic lens, cylindrical lens and mechanical slits were purchased from Zolix. 488 nm laser was purchased from Fiber Laser Technology.

2.2. Preparation of Au nanoparticles and Au-BSA nanoparticles

The Au nanoparticles (NPs) were prepared using the kinetically controlled seeded growth method [31]. Briefly, 150 mL of sodium citrate (2.2 mM) was heated in a 250 mL three-necked round-bottomed flask under vigorous stirring, which was followed by injection of 1 mL of HAuCl_4 (25 mM) once boiled. The color of the solution changed from yellow to bluish gray and then to soft pink after 15 min heating. Then, 1 mL of sodium citrate (60 mM) and 1 mL of a HAuCl_4 solution (25 mM) were sequentially injected (time delay ~ 2 min) to the solution for another 30 min heating. Au NPs were obtained once the solution was air-cooled down to room temperature. For surface modification of Au NPs, 25 mg BSA was added into 50 mL of as-prepared Au NPs solution. After 5 min of ultrasonic treatment, the mixture solution was put on a shaker and reaction was carried out for 1 h to form Au-BSA NPs.

2.3. Assessment of biocompatibility of Au/Au-BSA NPs

HMECs (2×10^4 cells in 0.1 mL ECM medium) were seeded into a 96-well culture plate and cultured overnight. Then the HMECs were treated with different concentrations of Au NPs or Au-BSA NPs (10, 20, 40 $\mu\text{g/mL}$) for 24 h and 48 h. After the treatment, HMECs were washed with PBS and then fresh ECM containing the CCK-8 reagent was added into the well. After incubated with CCK-8 reagent for 1.5 h, the absorption at 450 nm was measured using the microplate reader (Bio-Tek Synergy HT).

2.4. PC3 cells transfected with green fluorescent protein

A human prostate cancer PC3 cells, with high metastatic potential, were cultured in RPMI with 10% FBS. PC3 cells were seeded at a density of $3 \times 10^5/\text{mL}$ in 6-well plates with 1 mL of culture medium containing polybrene (6 $\mu\text{g/mL}$) and transfected with 2 μL of pLVX-EGFP1-C1

lentivirus vector containing green fluorescent protein (GFP) and the puromycin resistance gene. After transfection for 24 h, the medium was changed to fresh culture medium. The transfection efficiency of PC3-GFP cells evaluated using fluorescence microscope was above 95%. The highly bright PC3-GFP cells were selected by flow cytometry (FACS Aria II, Becton, Dickinson and Company) to establish tumor models.

2.5. Actin filaments staining

HMECs (2×10^5 cells in 1 mL ECM medium) were seeded into a 24-well culture plate and cultured for 48 h. Then the HMECs were treated with different concentrations of Au NPs (10, 20, 40 $\mu\text{g/mL}$), Au-BSA NPs (10, 20, 40 $\mu\text{g/mL}$) and EDTA (0.5 mM) for 1 h. Treated HMECs were fixed with 4% formaldehyde at room temperature for 15 min, and permeated with 0.1% Triton X-100 for 5 min. After rinsing with PBS, the treated HMECs were stained with 1 mL of phalloidin working solution, which was prepared by adding 1 μL of phalloidin conjugate DMSO solution to 1 mL of PBS with 1% BSA, for 1 h at room temperature. After gently rinsing 3 times with PBS to remove excess phalloidin conjugate, the HMECs were treated with 50 μL of antifade mounting medium (containing DAPI), which could stain the nucleus. Prepared HMECs were imaged by confocal microscope (Leica, SP8). DAPI channel (Ex: 405 nm, Em: 420 - 500 nm), phalloidine channel (Ex: 561 nm, Em: 580 - 650 nm). Three actin fluorescence images were randomly selected, and the area of gaps between the HMECs was measured by ImageJ.

2.6. Extravasation assay

0.9 mL and 0.1 mL of ECM were added to lower chamber and upper insert to prewet the inserts, respectively. The HMECs (2×10^4 cells in 0.1 mL ECM medium) were seeded in the transwell inserts with core size of 8 μm and cultured for 48 h to form a confluent monolayer, which could mimic the actual vascular wall. Then the HMECs were treated with different concentrations of Au NPs (10, 20, 40 $\mu\text{g/mL}$), Au-BSA NPs (10, 20, 40 $\mu\text{g/mL}$) and EDTA (0.5 mM) for 1 h. After treatment, PC3-GFP cells (4×10^4 cells suspended in 200 μL serum-free medium) were added into the upper inserts and cultured for another 24 h. The upper inserts were removed and the migrated PC3-GFP cells in the lower chamber were imaged by confocal microscope (Leica, SP8). GFP channel (Ex: 488 nm, Em: 500 - 550 nm). Three areas were randomly selected for imaging and the number of PC3-GFP cells in lower chamber was counted and analyzed.

2.7. Mouse model

All the animal care and experimental procedures were approved by the Ethical Committee of Animal Experiments in the School of Biomedical Engineering, Shanghai Jiao Tong University. Male BALB/c nude mice (6 weeks old) were purchased from Shanghai Slake Laboratory Animal Co., LTD. To establish the model of prostate cancer, PC3-GFP cells (1×10^6) were subcutaneously injected in the armpit of male BALB/c nude mice. Once the tumor volume reached about 100 mm^3 , the mice were randomly divided into three groups i.e. control, Au NPs and Au-BSA NPs groups ($n = 5$) for in vivo metastasis studies. The weight and tumor volume of mice were measured every other day. The tumor sizes were measured by a vernier caliper ruler and calculated using the formula (tumor volume = (length \times width 2)/2).

2.8. Injection of NPs and detection of CTCs

The mice in NPs treatment groups were injected with 10 mg kg^{-1} Au NPs or Au-BSA NPs via tail vein from Day 0, ten times administration of NPs were performed for the whole experiment, while mice in control group were injected with the equal volume of PBS. The detection of CTCs by IVFC was carried out every week i.e. Day 7, Day 14 and Day 21. After anesthetized and subsequently placed on the customized board with ear spreading on the glass slide, the CTCs of tumor-bearing mouse were monitored using IVFC for 30 min (three blood vessels were selected

for CTCs monitoring and each blood vessel was monitored for 10 min). The experimental procedure details are shown in Fig. 1.

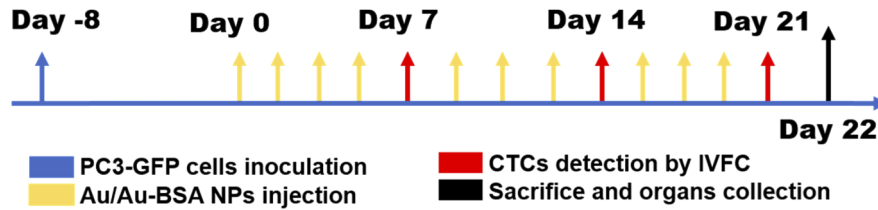


Fig. 1. The experimental procedure of in vivo CTCs detection.

2.9. Imaging of metastatic sites on organs

After in vivo study of NPs promoted cancer metastasis, the mice from both control and NPs treated groups were sacrificed and the major organs including heart, liver, spleen, lung, kidney were collected for metastases study via monitoring the green fluorescence signal from the metastasized PC3-GFP cells using in vivo fluorescence imaging system (PerkinElmer, IVIS Lumina LT).

2.10. Optical system for CTCs detection

The in vivo flow cytometry (IVFC) was set up to noninvasively detect the metastasized PC3-GFP cells as shown in Fig. 2. Briefly, light emitting diode (LED, 535 ± 15 nm) and charge-coupled device (CCD) were employed to illuminate and visualize the major veins and arteries of ear

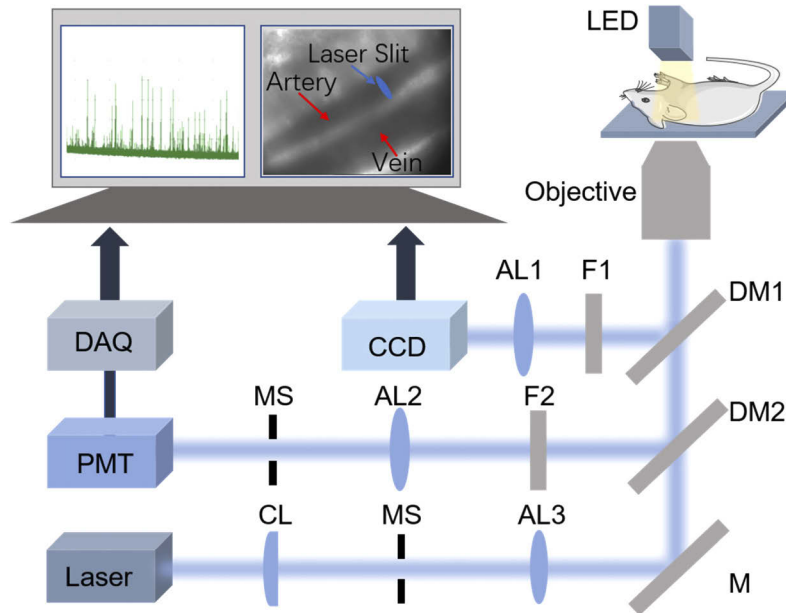


Fig. 2. The schematic diagram of the optical system for in vivo cancer metastasis study. CL: cylindrical lens; MS: mechanical slit; AL: achromatic lens; M: mirror; DM1: dichroic mirror (75% transmission and 25% reflection); DM2: dichroic mirror (488 nm transmission and 510 nm reflection); F1, F2: bandpass filter (510 ± 10 nm); Objective lens (40 \times , NA=0.6); DAQ: data acquisition; Laser: 488 nm.

microcirculation. The light emitted from 488 nm laser was focused into a slit by a cylindrical lens and further focused using objective lens (40 \times , NA = 0.6), and consequently cross the ear artery, which diameter was around 50 μ m. Once flow through this slit, the metastasized PC3-GFP cells were excited and emitted fluorescence of GFP, which was collected by objective lens and detected by a photomultiplier tube (PMT) placed directly behind the mechanical slit and the spectral filter for GFP.

2.11. Statistical analysis

All data were presented as mean \pm SD. Statistical analysis of data utilized the unpaired Student's t-test by GraphPad Prism 8.

3. Results and discussion

3.1. Characterization of Au nanoparticles

Gold has been widely used to construct photothermal agent, biosensors, surface-enhanced Raman scattering probes, etc., for cancer theranostics [32–37]. Moreover, gold and gold-based nanoparticles (NPs) are currently used for clinical applications, making gold promising in biomedical and clinical fields [38]. Thus the Au NPs, which were synthesized by a kinetically controlled seeded growth method [31], were selected to investigate the influence of NPs on cancer metastasis. During the growth, the absorption spectra of synthesized Au NPs were characterized as shown in Fig. 3(a). Compared with Au seeds, the absorption peak of Au NPs shifted to the longer wavelength, which was consistent with previous reports [31]. Then the Au NPs with absorption peak located at 524 nm were selected for the following studies. The size of Au NPs was measured as \sim 25 nm, which was beneficial for biomedical applications, by DLS measurement as shown in Fig. 3(b). In order to improve the biocompatibility and stability in biological media, the Au NPs were encapsulated with BSA to form Au-BSA NPs. Then the size distribution and mean size of Au and Au-BSA NPs in water and ECM were measured as shown in Fig. 3(b). It was found that Au NPs in ECM became remarkably larger than that in water, which can be attributed to that biomolecules of ECM conjugated to the abundant surface functional groups of Au NPs. Meanwhile, the size of Au-BSA NPs in ECM was similar as that in water, indicating the good stability in biological media. The biocompatibility of Au/Au-BSA NPs was evaluated by CCK-8 assay before carrying out in vitro and in vivo experiments. As shown in Fig. 3(c), there was no any significant difference between control cells and cells treated with Au/Au-BSA NPs for 24 and 48 h, indicating the excellent biocompatibility of Au/Au-BSA NPs.

3.2. Mechanism studies of NPs promoted cancer metastasis

Before performing in vivo detection of cancer metastasis, the mechanism of NPs promoted cancer metastasis was studied in vitro. It has been reported that nanomaterials-induced endothelial leakiness (NanoEL) [14], which might be beneficial for the intravasation of surviving cancer cells into the surrounding vasculature and subsequently extravasation, could promote cancer metastasis. Thus, the integrity of endothelial cells and endothelial cell-cell interactions were investigated using fluorescence imaging methods. After treated with different concentrations of Au/Au-BSA NPs for 1 h, HMECs were incubated with DAPI and phalloidine to co-stain nucleus and actin. As shown in Fig. 4(a), intracellular stress fibers of control and Au/Au-BSA NPs treated HMECs were almost similar, indicating the intact of endothelial cells and eliminating the toxicity interference. However, pericellular actin fibers showed a dose-dependent manner, with increment of NPs dose, and pericellular actin fibers were less evenly distributed and more gap regions appeared (yellow boxes in Fig. 4(a)), which were statistically analyzed in Fig. 4(b). It means that NPs disrupted endothelial cell-cell interactions and subsequently NanoEL provided the channel for cancer metastasis.

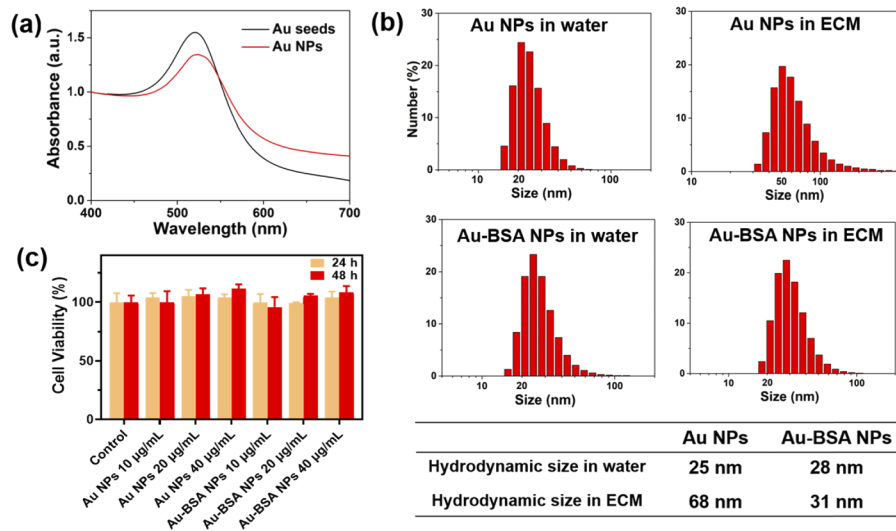


Fig. 3. (a) The absorption curves of Au seeds and Au NPs. (b) The size distribution and statistics of mean size of Au NPs and Au-BSA NPs in water and ECM culture medium. (c) Cell viability of control cells and Au/Au-BSA NPs treated cells for 24 h and 48 h. The data were presented as mean \pm SD ($n = 3$).

In order to further study whether the formed gaps by NanoEL could promote the cancer metastasis, the cancer cells migration across the endothelial monolayer treated with/without NPs was measured using extravasation assay. After HMECs were treated with various concentrations of Au/Au-BSA NPs or EDTA (positive control group), the migrated PC3-GFP cells were imaged as shown in Fig. 5(a). It was observed that the cellular migration of NPs treated groups lied between the EDTA-treated positive control group and blank control group as shown in Fig. 5(b), meanwhile the NPs resulted in a dose-dependent migration of PC3-GFP cancer cells across the endothelial barrier, which was consistent with phenomenon mentioned in Fig. 4. Moreover, the cellular migration of Au-BSA NPs treated groups was smaller than that of Au NPs treated groups, which might be attributed to the improved biocompatibility and stability endowed by encapsulation. Thus, it can be concluded that the cancer cells could exploit the intercellular gaps induced by NanoEL to cross the compromised endothelial monolayer, facilitating cancer metastasis.

3.3. *In vivo investigation of NPs promoted metastasis*

The tumor-bearing mouse model was established by subcutaneously injecting PC3-GFP cells (10^6 cells in 100 μ L culture medium without FBS) in the armpit of nude mouse. When the tumor volume reached 100 mm^3 , the mice were randomly divided into three groups ($n = 5$), i.e. Au NPs group, Au-BSA NPs group and blank control group. The mice in Au NPs group and Au-BSA NPs group were respectively injected with 10 mg kg^{-1} Au NPs and Au-BSA NPs 10 times, while the mice in blank control group were injected with same volume of PBS, and the CTCs of all mice were in vivo monitored by in vivo flow cytometry (IVFC) every week. After anesthetized, the mice were positioned onto the stage, and then the artery in the ear was excited by the 488 nm laser slit as shown in Fig. 6(a). Once the PC3-GFP cancer cells permeated into the surrounding vasculature and subsequently reached the laser slit of the selected artery, the fluorescence signal of the PC3-GFP cells i.e. CTCs, as the marker of cancer metastasis, could be detected as shown in Fig. 6(b), and one detected signal of CTC was enlarged as shown in Fig. 6(c).

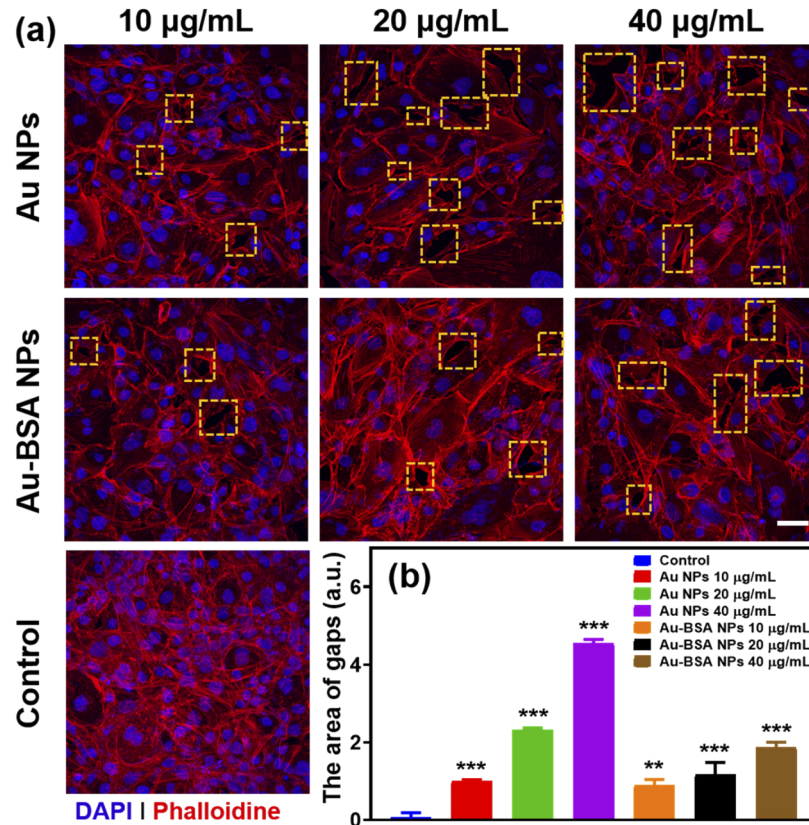


Fig. 4. (a) Representative nucleus/actin fluorescence images of control, Au/Au-BSA NPs-treated HMECs. Yellow boxes indicated gap regions between HMECs. DAPI channel (Ex: 405 nm, Em: 420 - 500 nm), phalloidine channel (Ex: 561 nm, Em: 580 - 650 nm). Scale bar: 50 µm. (b) The statistical results of the gap area between HMECs in different groups. The data were presented as mean \pm SD (n = 3). Statistical comparison between control group and other groups, **P < 0.01, ***P < 0.001.

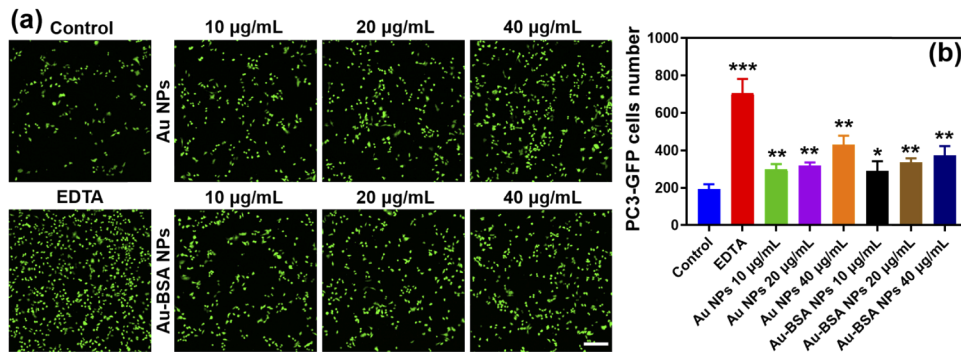


Fig. 5. (a) Fluorescence imaging and (b) statistical results of migrated PC3-GFP cancer cells crossed the compromised endothelial monolayer treated with NPs, EDTA. GFP channel (Ex: 488 nm, Em: 500 - 550 nm). Scale bar: 200 µm. The data were presented as mean \pm SD (n = 3). Statistical comparison between control group and other groups, *P < 0.05, **P < 0.01, ***P < 0.001.

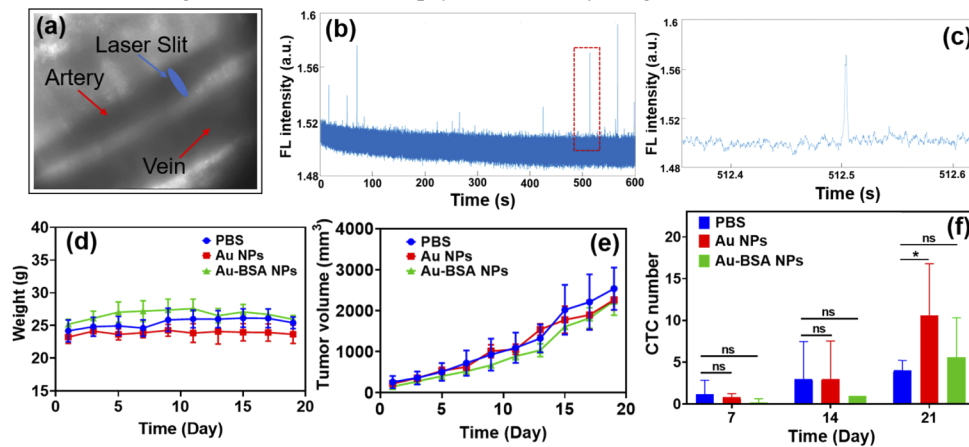


Fig. 6. (a) Bright field image of mouse ear blood vessel visualized using IVFC system. (b) Representative spectrum of circulating PC3-GFP cells in Au NPs group measured by IVFC. (c) The enlarged peak spectrum, indicating that one GFP-labeled PC3 cell passed through the light slit and emitted a burst of fluorescence. (d) The weight and (e) tumor volume of mice treated with Au/Au-BSA NPs or PBS. The data were presented as mean \pm SD ($n = 5$). (f) The measured CTC number of mice treated with Au/Au-BSA NPs or PBS by IVFC. The data were presented as mean \pm SD ($n = 5$), * $P < 0.05$, ns: no significant difference.

During the process of Au/Au-BSA NPs or PBS administration, the mice weight and tumor volume were recorded every other day. There was no significant body loss within 3 weeks as shown in Fig. 6(d), indicating that the administration of NPs would not affect the health conditions of mice. The tumor volume kept growing with similar increment rate for all groups as shown in Fig. 6(e), eliminating the inference on cancer metastasis from tumor size difference. Moreover, the CTCs of these mice were also in vivo and real-time monitored on Day 7, Day 14 and Day 21 as shown in Fig. 6(f). With increment of time, the CTC number kept growing for all groups, and there was no significant difference for CTC number among all groups at the early stage i.e. Day 7 and Day 14, indicating that low dose of NPs would not induce remarkable promotion of cancer metastasis. However, the CTC number of Au/Au-BSA treated group was significantly larger than that of blank control group at Day 21, indicating the NPs could promote the cancer metastasis due to NanoEL mechanism mentioned above. Meanwhile, CTC number of Au-BSA treated mice was less than that of Au treated mice, which might be attributed to improved biocompatibility and stability endowed by BSA encapsulation. The detected CTC number of different groups was in accordance with the migration rate of PC3-GFP cancer cells crossed the compromised endothelial monolayer treated with different NPs as shown in Fig. 5(b). Thus, it could be concluded that high dose of NPs can significantly promote the metastasis of prostate cancer, and encapsulation using biocompatible materials could alleviate cancer metastasis promoted by NPs. It was worth to note that neither any metastatic sites could be observed nor any CTCs could be measured in blood using conventional flow cytometry due to the extremely rare CTCs at early stage of metastasis, making IVFC a valuable biopsy tool for early diagnosis.

3.4. Ex vivo imaging of metastasis on organs

Considering that there were no metastatic sites on the mice body surface, the mice were sacrificed and the major organs (including heart, liver, spleen, lung, kidney) were collected to verify the promotion of cancer metastasis by Au NPs using fluorescence imaging method after in vivo investigation by IVFC. Since the metastases originated from CTCs escaped from primary tumor,

the metastases should express green fluorescence protein and emit bright green fluorescence. As shown in Fig. 7(a), the fluorescence images of major organs from different groups showed that the hearts from Au/Au-BSA NPs treated mice had obvious metastasis. In addition, the number of lung metastases of Au/Au-BSA NPs treated mice was significantly more than that of the control mice. The statistical results of the number of metastases were shown in Fig. 7(b). It was verified that high dose of Au NPs had a significant promotion on cancer metastasis of prostate cancer and Au-BSA NPs could alleviate promotion effect, which was consistent with the results measured by IVFC as shown in Fig. 6(f).

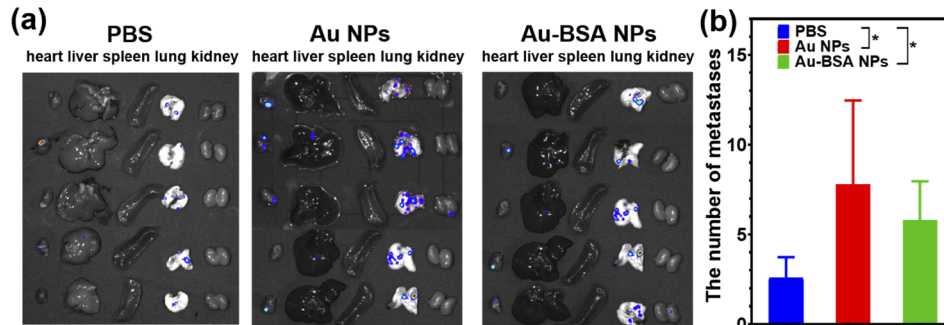


Fig. 7. (a) The fluorescence images of metastases on major organs (heart, liver, spleen, lung, kidney) of mice treated with Au/Au-BSA NPs and PBS. Ex: 500 nm slit. Em: 550 nm slit. (b) The statistical results of the metastases number. The data were presented as mean \pm SD (n = 5, *P < 0.05).

4. Conclusion

Nanomedicine was consciously designed for cancer treatment, but one side-effect, which could promote endothelial leakiness and cancer metastasis, was reported recently. However, there is no proper technology for noninvasive, real-time and in vivo monitoring of nanomaterials promoted cancer metastasis, limiting the nanomedicine optimization and screening. In order to bridge the gap, one new optical biopsy tool, i.e. in vivo flow cytometry (IVFC) was for the first time explored to study the relationship between nanoparticles and cancer metastasis. Both in vitro and in vivo experimental results demonstrated that the CTCs, the potential metastatic seeds, were Au nanoparticles dose-dependent, indicating the nanoparticles could promote cancer metastasis. It is worth to note that encapsulation of nanoparticle with biocompatible materials could alleviate the promotion effect. Moreover, the rare but significant CTCs couldn't be monitored using common methods at the early stage of cancer metastasis, endowing IVFC a great potential in fundamental, pre-clinical and clinical investigation of nanomaterials and cancer metastasis.

Funding. National Key Research and Development Program of China (2019YFC1604604); National Natural Science Foundation of China (61805135, 62027824); Shanghai Jiao Tong University (ZH2018QNA43).

Acknowledgments. This work was supported by the National Key Research and Development Program of China (2019YFC1604604), the Natural Science Foundation of China (61805135, 62027824), Shanghai Jiao Tong University (ZH2018QNA43).

Disclosures. The authors declare no conflicts of interest.

References

1. F. Bray, J. Ferlay, I. Soerjomataram, R. L. Siegel, L. A. Torre, and A. Jemal, "Global cancer statistics 2018: GLOBOCAN estimates of incidence and mortality worldwide for 36 cancers in 185 countries," *CA-Cancer J. Clin.* **68**(6), 394–424 (2018).

2. P. Agostinis, K. Berg, K. A. Cengel, T. H. Foster, A. W. Girotti, S. O. Gollnick, S. M. Hahn, M. R. Hamblin, A. Juzeniene, D. Kessel, M. Korbelik, J. Moan, P. Mroz, D. Nowis, J. Piette, B. C. Wilson, and J. Golab, "Photodynamic therapy of cancer: an update," *CA-Cancer J. Clin.* **61**(4), 250–281 (2011).
3. F. Yin, B. Gu, Y. N. Lin, N. Panwar, S. C. Tjin, J. L. Qu, S. P. Lau, and K. T. Yong, "Functionalized 2D nanomaterials for gene delivery applications," *Coordin. Chem. Rev.* **347**, 77–97 (2017).
4. Y. J. Liu, P. Bhattarai, Z. F. Dai, and X. Y. Chen, "Photothermal therapy and photoacoustic imaging via nanotheranostics in fighting cancer," *Chem. Soc. Rev.* **48**(7), 2053–2108 (2019).
5. B. Gu, W. B. Wu, G. X. Xu, G. X. Feng, F. Yin, P. H. J. Chong, J. L. Qu, K. T. Yong, and B. Liu, "Precise two-photon photodynamic therapy using an efficient photosensitizer with aggregation-induced emission characteristics," *Adv. Mater.* **29**(28), 1701076 (2017).
6. H. Y. Fan, X. H. Yu, K. Wang, Y. J. Yin, Y. J. Tang, Y. L. Tang, and X. H. Liang, "Graphene quantum dots (GQDs)-based nanomaterials for improving photodynamic therapy in cancer treatment," *Eur. J. Med. Chem.* **182**, 111620 (2019).
7. L. Qin, S. S. Jiang, H. Y. He, G. X. Ling, and P. Zhang, "Functional black phosphorus nanosheets for cancer therapy," *J. Control Release* **318**, 50–66 (2020).
8. W. Pang, P. F. Jiang, S. H. Ding, Z. Z. Bao, N. T. Wang, H. X. Wang, J. L. Qu, D. Wang, B. Gu, and X. B. Wei, "Nucleolus-targeted photodynamic anticancer therapy using renal-clearable carbon dots," *Adv. Healthcare Mater.* **9**(16), 2000607 (2020).
9. Y. Y. Jiang, J. C. Li, X. Zhen, C. Xie, and K. Y. Pu, "Dual-peak absorbing semiconducting copolymer nanoparticles for first and second near-infrared window photothermal therapy: a comparative study," *Adv. Mater.* **30**(14), 1705980 (2018).
10. X. J. Cheng, R. Sun, L. Yin, Z. F. Chai, H. B. Shi, and M. Y. Gao, "Light-triggered assembly of gold nanoparticles for photothermal therapy and photoacoustic imaging of tumors in vivo," *Adv. Mater.* **29**(6), 1604894 (2017).
11. P. Yang, S. Zhang, N. Zhang, Y. Wang, J. Zhong, X. X. Sun, Y. Qi, X. F. Chen, Z. Li, and Y. W. Li, "Tailoring synthetic melanin nanoparticles for enhanced photothermal therapy," *ACS Appl. Mater. Interfaces* **11**(45), 42671–42679 (2019).
12. M. Babaei, H. Eshghi, K. Abnous, M. Rahimizadeh, and M. Ramezani, "Promising gene delivery system based on polyethylenimine-modified silica nanoparticles," *Cancer Gene Ther.* **24**(4), 156–164 (2017).
13. C. M. Hartshorn, M. S. Bradbury, G. M. Lanza, A. E. Nel, J. H. Rao, A. Z. Wang, U. B. Wiesner, L. Yang, and P. Grodzinski, "Nanotechnology strategies to advance outcomes in clinical cancer care," *ACS Nano* **12**(1), 24–43 (2018).
14. F. Peng, M. I. Setyawati, J. K. Tee, X. G. Ding, J. P. Wang, M. E. Nga, H. K. Ho, and D. T. Leong, "Nanoparticles promote in vivo breast cancer cell intravasation and extravasation by inducing endothelial leakiness," *Nat. Nanotechnol.* **14**(3), 279–286 (2019).
15. G. P. Gupta and J. Massague, "Cancer metastasis: building a framework," *Cell* **127**(4), 679–695 (2006).
16. Z. Y. Shen, A. G. Wu, and X. Y. Chen, "Current detection technologies for circulating tumor cells," *Chem. Soc. Rev.* **46**(8), 2038–2056 (2017).
17. P. G. Schiro, M. X. Zhao, J. S. Kuo, K. M. Koehler, D. E. Sabath, and D. T. Chiu, "Sensitive and high-throughput isolation of rare cells from peripheral blood with ensemble-decision aliquot ranking," *Angew. Chem. Int. Ed.* **51**(19), 4618–4622 (2012).
18. M. Y. Sha, H. X. Xu, M. J. Natan, and R. Cromer, "Surface-enhanced raman scattering tags for rapid and homogeneous detection of circulating tumor cells in the presence of human whole blood," *J. Am. Chem. Soc.* **130**(51), 17214–17215 (2008).
19. Y. Wan, M. Winter, B. Delalat, J. E. Hardingham, P. K. Grover, J. Wrin, N. H. Voelcker, T. J. Price, and B. Thierry, "Nanostructured polystyrene well plates allow unbiased high-throughput characterization of circulating tumor cells," *ACS Appl. Mater. Interfaces* **6**(23), 20828–20836 (2014).
20. S. B. Cheng, M. Xie, J. Q. Xu, J. Wang, S. W. Lv, S. Guo, Y. Shu, M. Wang, W. G. Dong, and W. H. Huang, "High-efficiency capture of individual and cluster of circulating tumor cells by a microchip embedded with three-dimensional poly(dimethylsiloxane) scaffold," *Anal. Chem.* **88**(13), 6773–6780 (2016).
21. J. Kim, H. Cho, S. I. Han, and K. H. Han, "Single-cell isolation of circulating tumor cells from whole blood by lateral magnetophoretic microseparation and microfluidic dispensing," *Anal. Chem.* **88**(9), 4857–4863 (2016).
22. H. Y. Zhang, Z. Z. Jia, C. C. Wu, L. G. Zang, G. W. Yang, Z. Z. Chen, and B. Tang, "In vivo capture of circulating tumor cells based on transfusion with a vein indwelling needle," *ACS Appl. Mater. Interfaces* **7**(36), 20477–20484 (2015).
23. P. Kim, E. Chung, H. Yamashita, K. E. Hung, A. Mizoguchi, R. Kucherlapati, D. Fukumura, R. K. Jain, and S. H. Yun, "In vivo wide-area cellular imaging by side-view endomicroscopy," *Nat. Methods* **7**(4), 303–305 (2010).
24. H. Seo, Y. Hwang, K. Choe, and P. Kim, "In vivo quantitation of injected circulating tumor cells from great saphenous vein based on video-rate confocal microscopy," *Biomed. Opt. Express* **6**(6), 2158–2167 (2015).
25. K. Tanaka, Y. Toiyama, Y. Okugawa, M. Okigami, Y. Inoue, K. Uchida, T. Araki, Y. Mohri, A. Mizoguchi, and M. Kusunoki, "In vivo optical imaging of cancer metastasis using multiphoton microscopy: a short review," *Am. J. Transl. Res.* **6**, 179–187 (2014).
26. E. I. Galanzha, Y. A. Menyayev, A. C. Yadem, M. Sarimollaoglu, M. A. Juratli, D. A. Nedosekin, S. R. Foster, A. Jamshidi-Parsian, E. R. Siegel, I. Makhoul, L. F. Hutchins, J. Y. Suen, and V. P. Zharov, "In vivo liquid biopsy using

- Cytophone platform for photoacoustic detection of circulating tumor cells in patients with melanoma," *Sci. Transl. Med.* **11**(496), eaat5857 (2019).
27. I. Georgakoudi, N. Solban, J. Novak, W. L. Rice, X. B. Wei, T. Hasan, and C. P. Lin, "In vivo flow cytometry: a new method for enumerating circulating cancer cells," *Cancer Res.* **64**(15), 5044–5047 (2004).
 28. D. A. Nedosekin, M. Sarimollaoglu, E. I. Galanzha, R. Sawant, V. P. Torchilin, V. V. Verkhusha, J. Ma, M. H. Frank, A. S. Biris, and V. P. Zharov, "Synergy of photoacoustic and fluorescence flow cytometry of circulating cells with negative and positive contrasts," *J. Biophotonics* **6**(5), 425–434 (2013).
 29. N. A. Koonce, M. A. Juratli, C. Cai, M. Sarimollaoglu, Y. A. Menyaev, J. Dent, C. M. Quick, R. P. Dings, D. Nedosekin, and V. Zharov, "Real-time monitoring of circulating tumor cell (CTC) release after nanodrug or tumor radiotherapy using in vivo flow cytometry," *Biochem. Biophys. Res. Commun.* **492**(3), 507–512 (2017).
 30. M. A. Juratli, M. Sarimollaoglu, E. R. Siegel, D. A. Nedosekin, E. I. Galanzha, J. Y. Suen, and V. P. Zharov, "Real-time monitoring of circulating tumor cell release during tumor manipulation using in vivo photoacoustic and fluorescent flow cytometry," *Head Neck* **36**(8), 1207–1215 (2014).
 31. N. G. Bastus, J. Comenge, and V. Puentes, "Kinetically controlled seeded growth synthesis of citrate-stabilized gold nanoparticles of up to 200 nm: size focusing versus ostwald ripening," *Langmuir* **27**(17), 11098–11105 (2011).
 32. S. M. Shawky, A. M. Awad, W. Allam, M. H. Alkordi, and S. F. El-Khamisy, "Gold aggregating gold: a novel nanoparticle biosensor approach for the direct quantification of hepatitis C virus RNA in clinical samples," *Biosens. Bioelectron.* **92**, 349–356 (2017).
 33. J. Nam, S. Son, L. J. Ochyl, R. Kuai, A. Schwendeman, and J. J. Moon, "Chemo-photothermal therapy combination elicits anti-tumor immunity against advanced metastatic cancer," *Nat. Commun.* **9**(1), 1074 (2018).
 34. L. Zhou, J. Zhou, W. Lai, X. D. Yang, J. Meng, L. B. Su, C. J. Gu, T. Jiang, E. Y. B. Pun, L. Y. Shao, L. Petti, X. W. Sun, Z. H. Jia, Q. X. Li, J. G. Han, and P. Mormile, "Irreversible accumulated SERS behavior of the molecule-linked silver and silver-doped titanium dioxide hybrid system," *Nat. Commun.* **11**(1), 1785 (2020).
 35. L. R. Hirsch, R. J. Stafford, J. A. Bankson, S. R. Sershen, B. Rivera, R. E. Price, J. D. Hazle, N. J. Halas, and J. L. West, "Nanoshell-mediated near-infrared thermal therapy of tumors under magnetic resonance guidance," *Proc. Natl. Acad. Sci. U. S. A.* **100**(23), 13549–13554 (2003).
 36. V. P. Zharov, V. Galitovsky, and M. Viegas, "Photothermal detection of local thermal effects during selective nanophotothermolysis," *Appl. Phys. Lett.* **83**(24), 4897–4899 (2003).
 37. J. Shao, R. J. Griffin, E. I. Galanzha, J. W. Kim, N. Koonce, J. Webber, T. Mustafa, A. S. Biris, D. A. Nedosekin, and V. P. Zharov, "Photothermal nanodrugs: potential of TNF-gold nanospheres for cancer theranostics," *Sci. Rep.* **3**(1), 1293 (2013).
 38. A. R. Rastinehad, H. Anastos, E. Wajswol, J. S. Winoker, J. P. Sfakianos, S. K. Doppalapudi, M. R. Carrick, C. J. Knauer, B. Taouli, S. C. Lewis, A. K. Tewari, J. A. Schwartz, S. E. Canfield, A. K. George, J. L. West, and N. J. Halas, "Gold nanoshell-localized photothermal ablation of prostate tumors in a clinical pilot device study," *Proc. Natl. Acad. Sci. U.S.A.* **116**(37), 18590–18596 (2019).